***Soil tests***

**(1) In-situ test**

In order to sound the strength of the soils in Las Colinas Mountain, portable cone penetration tests (Japan Geotechnical Society, 1995) were performed at three points **C1-C3** in **Figure 2.30**. Among them, Point **C1** is located slightly west off the main scarp. The equipment is made up of a pair of rods coupled upright with a knocking head. A cone is attached to its bottom end, and a hammer drops down along a guide groove cut straight on the surface of the upper rod (**Figure 2.31**).

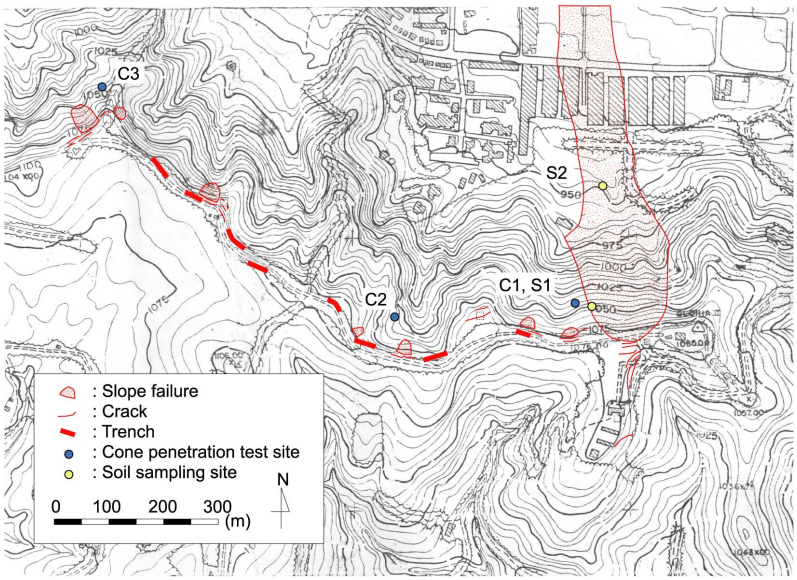


**Point S1**

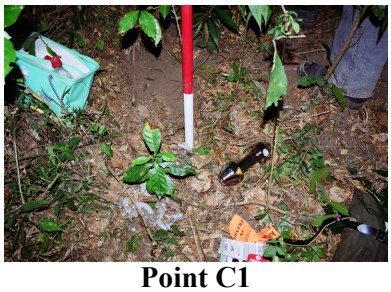

**Point C1**

**Point C3**

**Figure 2.30** (same as **Figure 2.12**). Points of soil sounding (**C1-C3**) and sampling (**S1**): CPT tests were performed at **C1**, **C2** and **C3** (dark blue dots), while soil samples were taken at S1 (yellow dot) for triaxial and ring-shear tests.

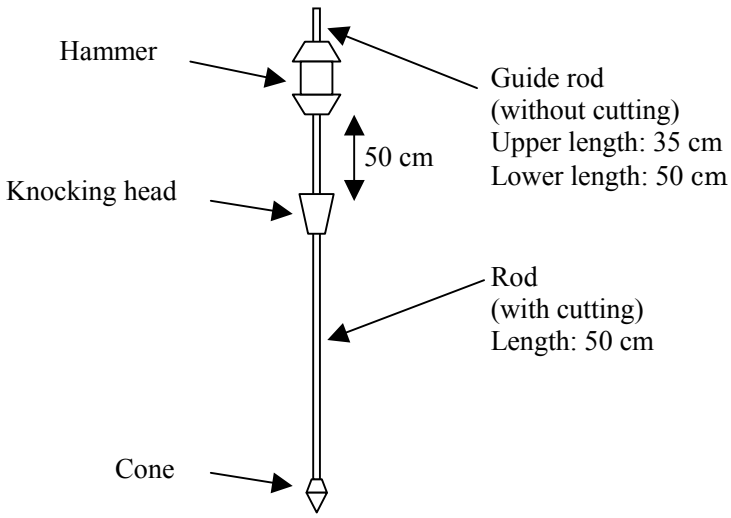


**Figure 2.31**. CPT Equipment

The procedure for the CPT testing follows:

1) Assemble the equipment.
2) Hold the equipment upright on a testing point.
3) Confirm that the hammer is never stuck in the groove, and drops smoothly along the guide rod.
4) When the equipment goes down under its own weight, record the depth that the cone has sunken. In this case, Nd (see the equation below) is set at 0. If not,
5) Drop the hammer from the height 50 cm above the knocking head. When the cone is driven about 10 cm deep, record the number of blows *N* and the exact depth *d* reached by this driving. Nd is then given by:

$$Nd = 10\frac{N}{d}$$

6) Stop the test when the depth after 10 times blows did not reach 2 cm.
7) Observe the soil when pulling out the equipment.

Positive correlation shown in the equation below is empirically recognized between Ns-values from standard penetration tests and Nd values from portable dynamic penetration tests

$$Ns = \frac{Nd}{1.5}$$

Variations with depth of the equivalent Ns-values at the three points are shown in **Figure 2.32**. As contrasted with other points, all equivalent Ns-values at Point C1 are considerably low as a whole. Among them, extremely low values reaching zero were found at about 1.2m and 2.5m depths. These two small Ns values suggest the presence of two weak layers, which can be the pumice and/or fragmental volcanic products judging from their depths.

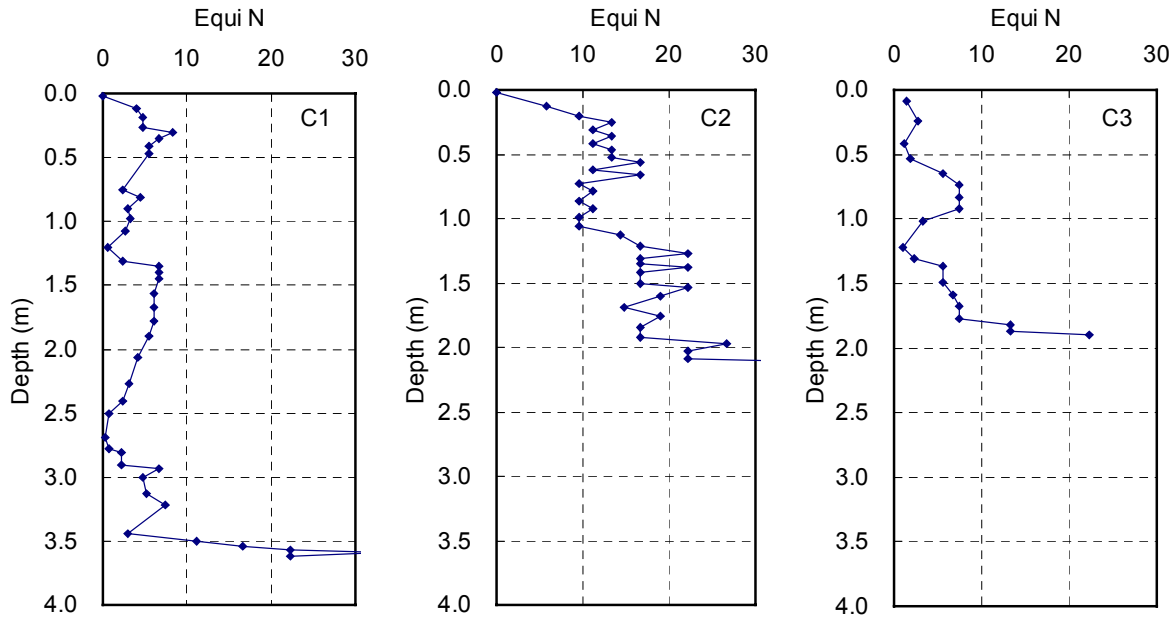


**Figure 2.32.** Equivalent Ns-values at three sites

**(2) Triaxial compression tests and ring shear tests**[*]

Such physical properties as static, dynamic and residual strengths of the pumice sand were examined in static and dynamic triaxial compression tests and ring shear tests. Samples of the pumice sand were taken from Point **S1** in **Figure 2.31** slightly below the west main scarp.

**Table 2.3** shows the measured properties of the pumice sand. Its density is comparably low as a sand. X-ray diffraction method detected that the pumice consists of plagioclase and glass (see **Figure 2.33**).

Static triaxial compression tests for the pumice sand of the natural water content of 40 % were carried out undrained after full consolidation. A specimen of 5 cm in diameter and 12 cm high was prepared by tamping. Mohr circles obtained from the tests are shown together with the inferred rupture envelope in **Figure 2.2.14**.

**Table 2.3** Physical properties of pumice soil

| $\rho_s$ (g/cm$^3$) | $D_{max}$ (mm) | $D_{50}$ (mm) | $F_c$ (%) | $U_c$ | $e_{max}$ | $e_{min}$ | Soil classification |
|---|---|---|---|---|---|---|---|
| 2.410 | 0.75 | 0.68 | 6.9 | 4.35 | 3.044 | 2.297 | S-V |

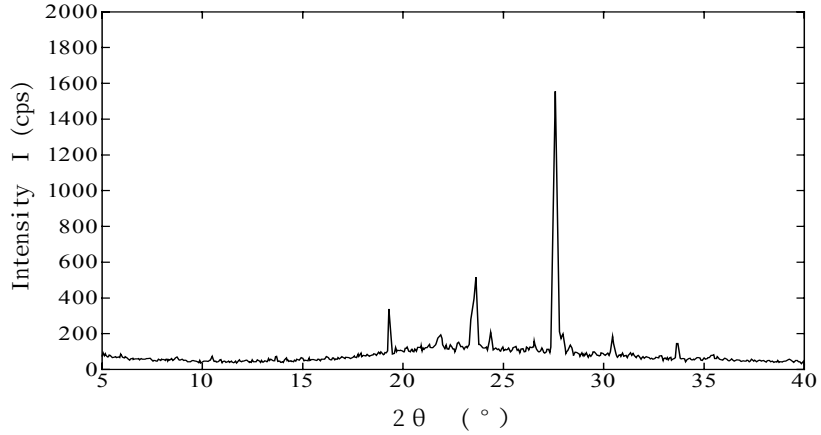


**Figure 2.33**. X-ray diffraction of the pumice soil

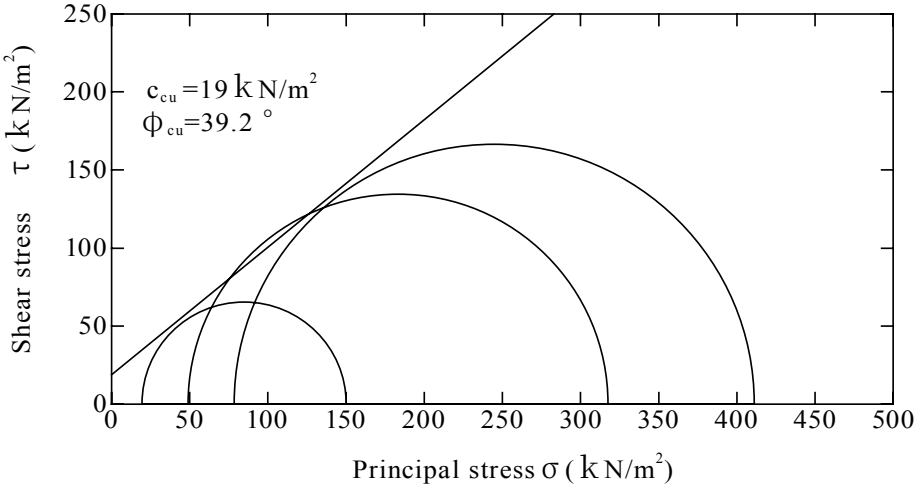


**Figure 2.34**. Mohr circles and the rupture line of pumice soil

[*] These tests were performed at Yamamoto laboratory, Yamaguchi University.

Dynamic triaxial compression (undrained) tests were performed on the same samples as those for the static triaxial compression tests after full consolidation. In addition, liquefaction resistance was examined after saturating specimens completely.

**Figures 2.35(a)** and **2.35(b)** show typical examples of time-varying strain and cyclic deviator stress ratio obtained from the dynamic triaxial tests for partly and fully saturated soil samples, respectively. Excessive pore pressure ratio is also shown in **Figure 2.35(b)**. **Figure 2.36** shows the relationship between different stress ratios and corresponding numbers of cycles required for the specimen to liquefy. A specimen was assumed to have liquefied when 5 % axial strain was reached in it.

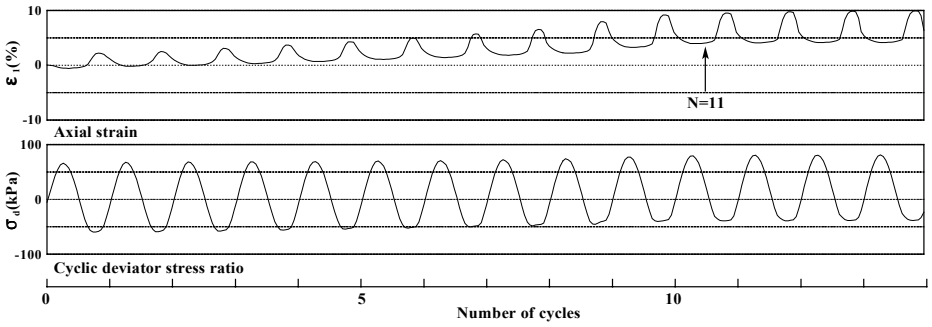


**(a)** Unsaturated pumice

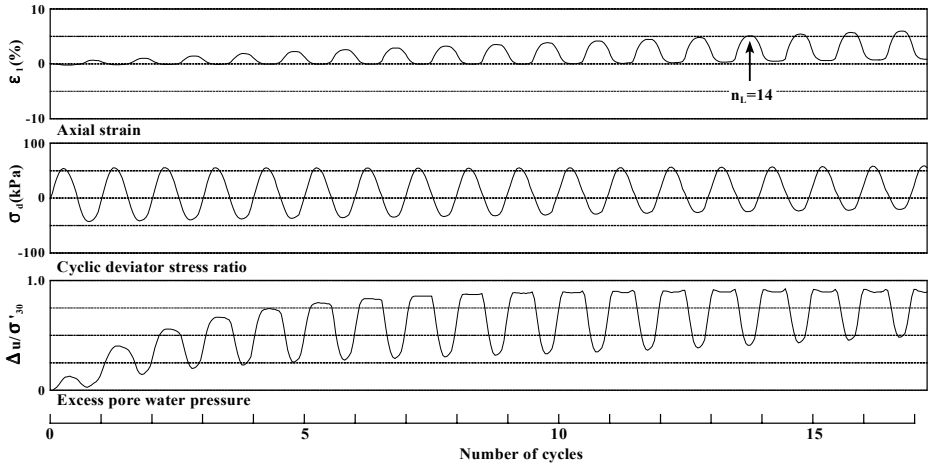


**(b)** Saturated pumice

**Figure 2.35**. Examples of time-varying strain and cyclic deviator stress ratio

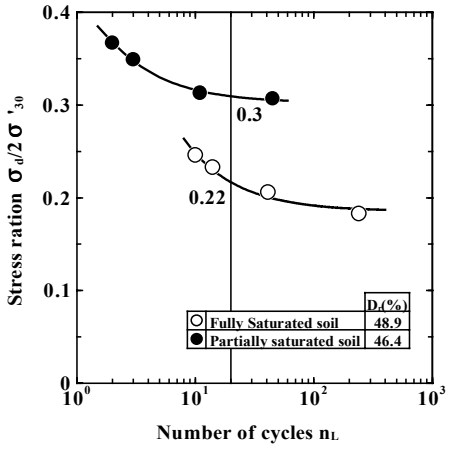


**Figure 2.36** Liquefaction strength

Ring shear tests were carried out on the same pumice sand of the natural water content. The maximum grain size included in the samples was 0.85 mm. The details of the ring shear testing apparatus (**Figure 2.37**) are available in a literature by Suzuki et al. (1997). The stress paths and the rupture envelope plotted in **Figure 2.38** show that the residual strength parameters $\phi_r$ and $c_r$ are 36.1° and 0 kPa, respectively. Measured strength parameters are summarized in **Table 2.4**.

**Figure 2.37**. Ring shear testing apparatus

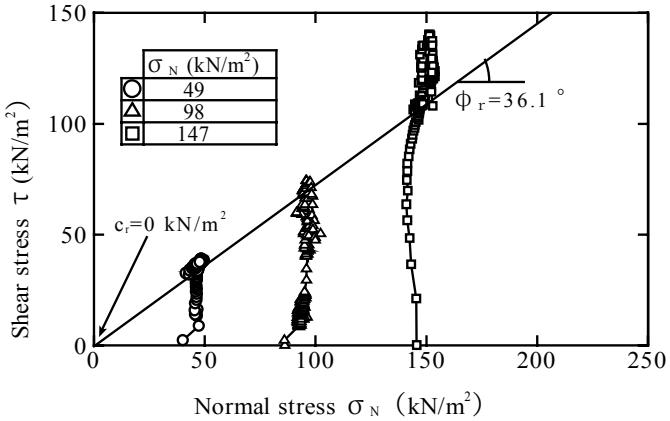


**Figure 2.38**. Stress paths and the rupture line of pumice soil

**Table 2.4**. Mechanical characteristics of pumice soil

| | |
|---|---|
| Static strength | $\phi_{cu}$=39.2 degrees, $c_{cu}$=19 kN/m$^2$ |
| Dynamic strength (partially saturated) | $(\sigma_d / 2\sigma'_{30})_{N=20}$=0.30 |
| Liquefaction strength (fully saturated) | $(\sigma_d / 2\sigma'_{30})_{N=20}$=0.22 |
| Residual strength (partially saturated) | $\phi_r$=36.1 degrees, $c_r$=0 kN/m$^2$ |

**Figures 2.39(a)** and **2.39(b)** are optical micrographs of the pumice grains before and after a static triaxial compression test. Fine contents of the pumice sand before and after a static triaxial test measured 6.90 % and 7.14 %, respectively. A pair of photos (**Figures 2.40(a)** and **2.40(b)**) compares grains shapes in the interior and exterior of the shear-band formed during a ring shear test. Grain crushing is clearly seen in the interior of the shear-band, while most grains are remaining uncrushed in its exterior.

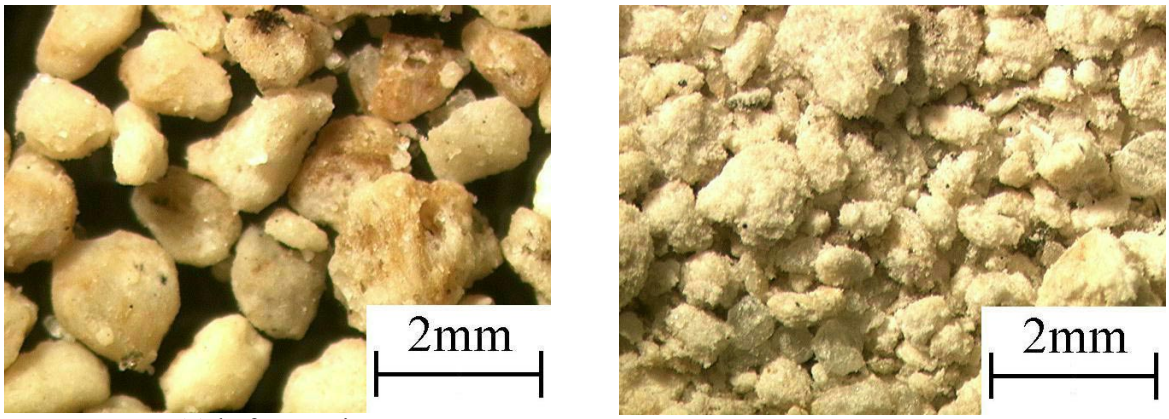


**(a)** before testing **(b)** after testing

**Figure 2.39**. Optical micrographs of pumice soil before and after static triaxial test

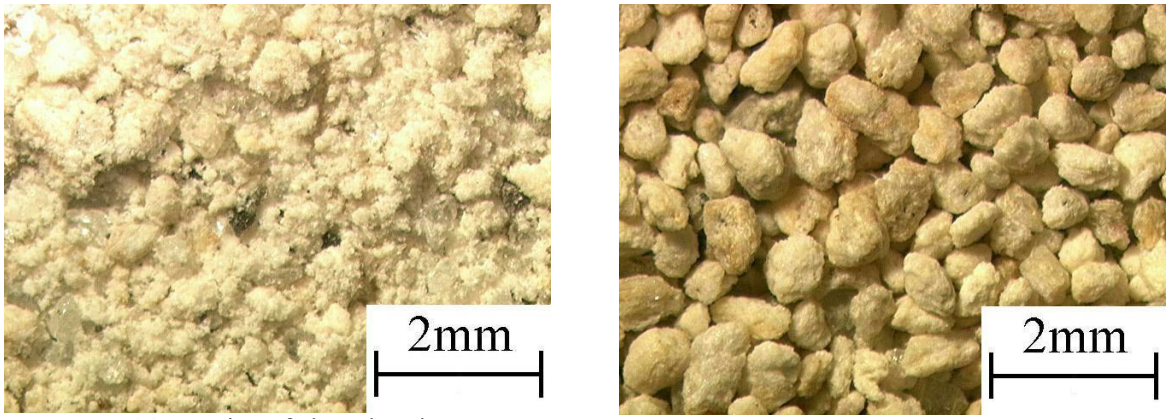


**(a)** Interior of shear band **(b)** Exterior of shear band

**Figure 2.40**. Optical micrographs of pumice soil in the interior and exterior of shearband

### (3) Ring shear tests*

The undrained ring shear apparatus (DPRI-5: **Figure 2.41**) was used to examine dynamic characteristics of the pumice in rapid shear (Sassa, 1998). Outer and inner diameters of the cylindrical shear box are 120 and 80 mm, respectively. The maximum shearing velocity of 10 cm/sec is realized within this box.

The concept of ring shear landslide simulation test is illustrated in **Figure 2.42** (Sassa, 2000). Shear/normal stresses along a sliding surface in place are realized in the interior of the shear box, and necessary physical quantities of the soil sample in shear (resistance, pore water pressure, shearing velocity and accordingly the mobilized apparent friction angle) are monitored in real time. An upright cross-section of the shear box with the pore pressure measuring system built in is shown in **Figure 2.43** (See Sassa (1998 and 2000) for further details).

**Table 2.5**. Mechanical properties of the sample

| Sample | **Pumice** |
|---|---|
| Mean grain size, $D_{50}$ (mm) | 0.91 |
| Effective grain size, $D_{10}$ (mm) | 0.25 |
| Uniformity coefficient, $U_c$ | 5.0 |
| Specific gravity, $G_s$ | 2.28 |

**Figure 2.41**. Ring shear apparatus

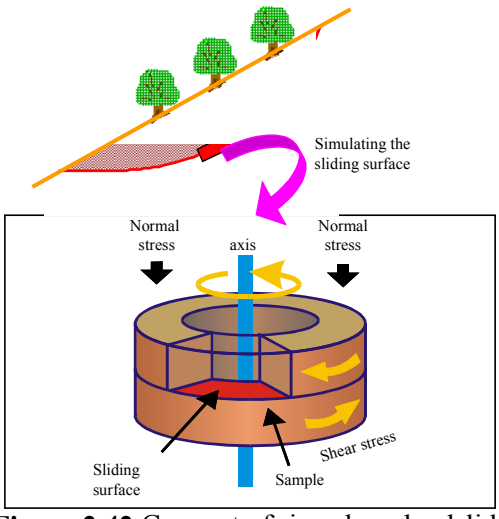


**Figure 2.42** Concept of ring shear landslide simulation test (Sassa, 2000)

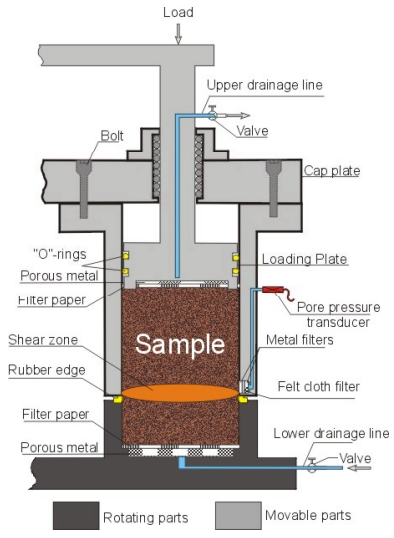


**Figure 2.43**. Schematic illustration of the section of undrained shear box (Sassa, 2000)

The shear box was first filled with oven-dried pumice sand, and after letting its entire voids be filled

* These tests wer performed at Sassa/Fukuoka Laboratory, DPRI, Kyoto University.

with $CO_2$ gas, the sand was saturated with de-aired water. Completion of saturation was checked with $B_D$ value (a pore pressure coefficient in direct shear proposed by Sassa (1985), and defined as the ratio of the pore pressure increment, Δu, and the normal stress increment, $\Delta\sigma$, namely $B_D = \Delta u/\Delta\sigma$). $B_D$ is calculated after consolidation and when $B_D$ falls in the range of 0.95-1.00, the sample is considered to be totally saturated. After the sample was normally or over consolidated, undrained shear tests were carried out under different shearing conditions.

Two ring shear tests were performed to examine the liquefaction possibility of the landslide soils with mechanical properties listed in **Table 2.5**. Samples with different saturation degrees (**TEST A**: $S_r$=100%, $B_D$=0.99, e=2.44; TEST B: $S_r$=81%, $B_D$=0.15, e= 2.45) were prepared, and normally consolidated under the stress state corresponding to a slope of 20° inclination. Shearing torque was controlled in both tests, and shear stresses were subsequently applied to the undrained samples at a loading rate of 0.098 kPa/sec after the consolidation. The sample was twisted off and began rotating when the stress state reached the failure line. Shearing was continued until 15-20 m displacement was reached.

**Figure 2.44(a)** shows the effective stress paths for the performed two tests (A and B). As soon as the shearing of the sample started in **TEST A (Sr=100%)**, there appeared an excessive pore pressure buildup, which was then followed by dilation of the pumice. When the residual failure line (RFL) was reached, a sudden decrease of apparent friction angle along the RFL was observed. The drop of the shear resistance is also plotted in **Figure 2.44(b)** with respect to the increasing shear displacement. When the twisted pumice sample had slipped 20m distance, the apparent friction angle of about 3.2 degrees was reached, the fact suggesting that a sliding-surface liquefaction occurred in the saturated soil sample (Sassa, 1996 and Sassa et al 1996). The average apparent friction angle mobilized in place, however, was seemingly about 13 degrees, much higher than 3.2 degrees reached in TEST A.

For this reason, **TEST B** was carried out for smaller value of Sr **(Sr =81%)**. In this test, the stress path went almost straight up until the RFL was reached (**Figure 2.44(a)**), and then the apparent friction angle dropped down to 12.7 degrees, which is closer to the angle roughly evaluated over the entire travel distance. The path deviated from the RFL presumably because the sensor did not keep a good track of pore pressure of the unsaturated pumice sample.

The RFL in **Figure 2.44(a)** was obtained after TEST A by the following procedure:

(a) The drainage valve on the top of the shear box was opened, and the pore pressure built up in the specimen was released.

(b) Normal stress was then gradually decreased at a constant rate of 0.2 kPa/sec to zero keeping the constant shearing speed of 0.2 mm/sec.

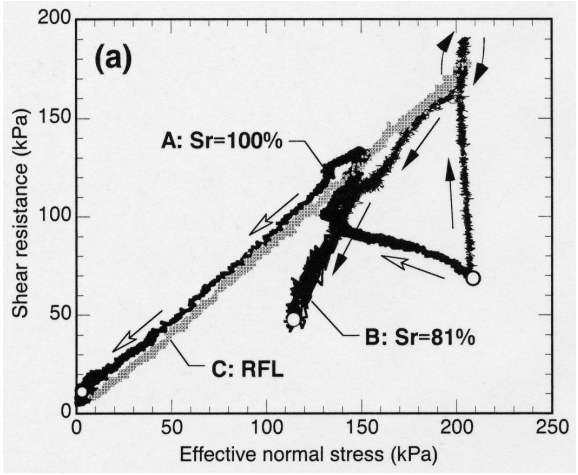


**(a)** Effective stress path

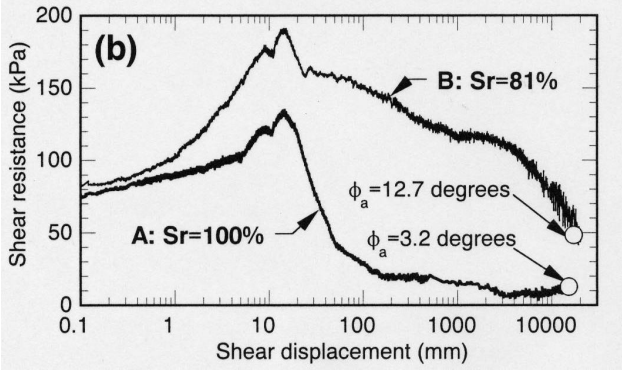


**(b)** Shear strength vs. shear displacement

**Figure 2.44**. Ring shear test results

Pairs of micrographs in **Figures 2.45** (optical) and **2.46** (SEM) compare microstructures of the pumice before and after the ring shear test. The scale is shown in each photo. Grain crushing due to shearing is obvious in each pair.


**Figure 2.45**. microstructure of the pumice by optical microscope
(Left: before the test, Right: after the test)

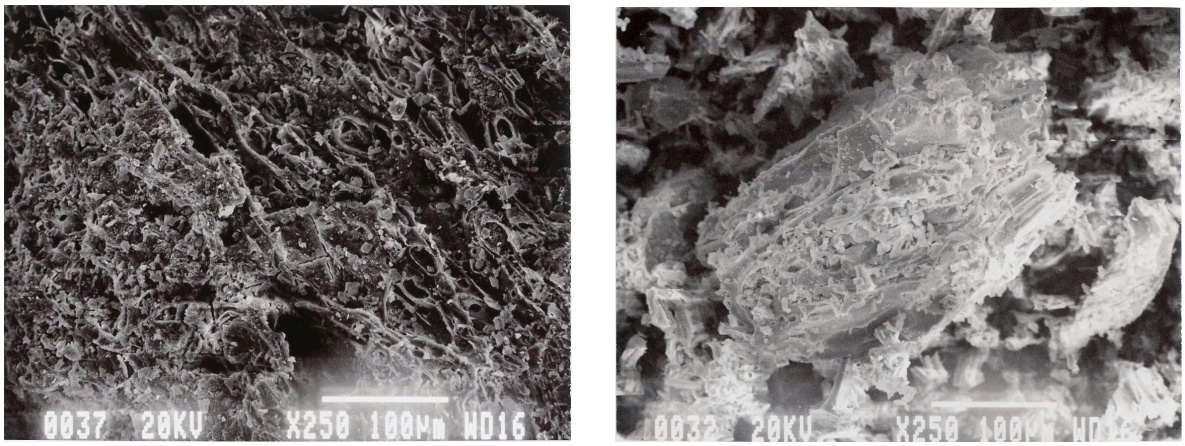


**(a)** 250 magnifications

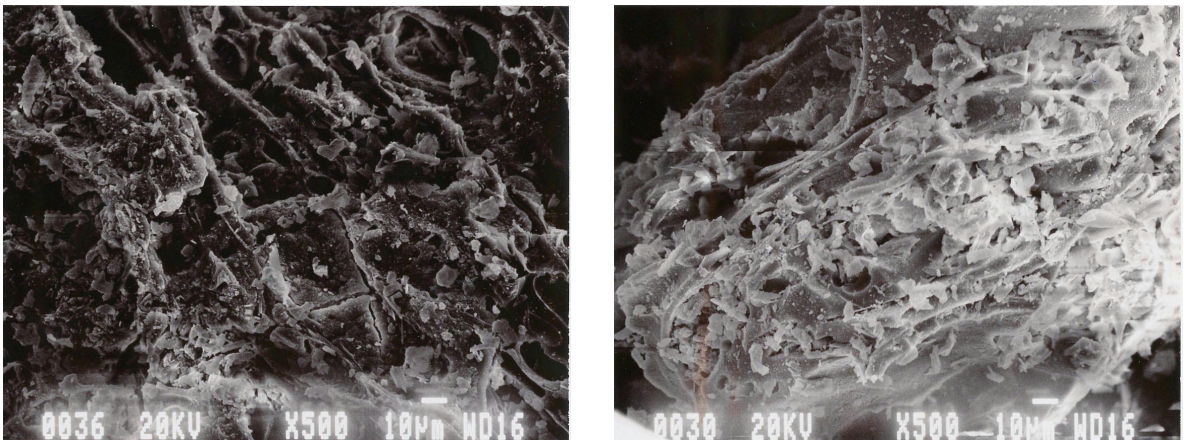


**(b)** 500 magnifications

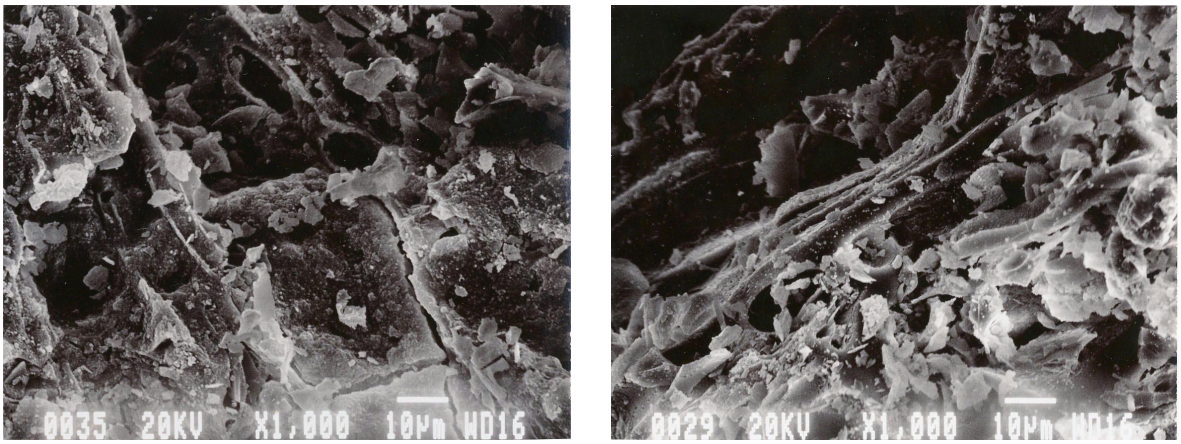


**(c)** 100 magnifications

**Figure 2.46**. microstructure of the pumice by SEM
(Left: before the test, Right: after the test)

to the next page